JOURNAL OF GUIDANCE, CONTROL, AND DYNAMICS
Vol. 32, No. 4, July–August 2009

Point Targeting of Multisatellites via a Virtual Structure Formation Flight Scheme

Chaeik Ahn* and Youdan Kim†
Seoul National University, Seoul 151-741, Republic of Korea

DOI: 10.2514/1.39537

This paper proposes a formation flight control scheme for spacecraft based on the virtual structure approach. The virtual structure approach treats the entire formation as a virtual rigid-body structure. With this approach, the geometric relationship among the spacecraft can be maintained during a maneuver. The information on the geometric relationships is used to complete the formation flight mission. Using rotational kinematics and rigid-body dynamics, the virtual structure formation algorithm calculates the reference position and attitude command to perform the synchronized maneuvers required to point to the desired target. The adaptive sliding mode control law is adopted to make the system track the reference command generated by the formation algorithm. An adaptive sliding mode controller, which combines the merits of the adaptive control scheme and the sliding mode control scheme, is proposed and used to make the spacecraft follow the specified position and attitude command. The stability of the proposed controller is analyzed by using the Lyapunov stability theorem, and a numerical simulation is performed to verify the effectiveness of the proposed formation algorithm and the adaptive sliding mode controller.

Nomenclature

$\mathbf{C}_i$	=	direction cosine matrix of satellite i
F	=	translational control forces
g	=	gravitational constant
h, β	=	positive sliding gain
$\hat{\mathbf{i}}$, $\hat{\mathbf{j}}$, $\hat{\mathbf{k}}$	=	unit vectors of local-vertical–local-horizontal frame
J	=	inertia of satellites
L_1, L_2, L_3	=	dimension of satellites
m	=	mass of satellites
$\mathbf{q}_v$	=	vector part of quaternion
$\mathbf{q}$	=	quaternion vector
$\tilde{\mathbf{q}}$	=	skew symmetric matrix of vector part of quaternion
$\Re$	=	orbit radius of reference satellite
S	=	sliding surface
$\mathbf{S}$	=	bore sight vector
sgn(·)	=	sign function
$\underline{\mathbf{u}}$	=	control vector
$\mathbf{u_f}$	=	thrust force vector
V_i	=	Lyapunov function candidate
υ	=	lumped uncertainty
X	=	centroid of virtual structure
x, y, z	=	positions in local-vertical–local-horizontal frame
$\mathbf{x}$	=	states vector
$\Delta(\cdot)$	=	uncertainties introduced by system parameters
θ	=	latitude angle of the reference satellite
μ	=	gravitational coefficient
ς	=	external disturbance
$\boldsymbol{\tau}$	=	control torques
$\tilde{\boldsymbol{\omega}}$	=	skew symmetric matrix of angular velocity vector
$\boldsymbol{\omega}$	=	angular velocity

Subscripts

b	=	body coordinate system
d	=	desired states
$i \times j$	=	$i \times j$ matrix

Superscripts

T	=	vector or matrix transpose
†	=	pseudoinverse of matrix

I. Introduction

FORMATION flying of spacecraft is considered to be a key technology for future space-based systems, because it allows one large expensive spacecraft to be replaced by a formation of smaller and cheaper spacecraft. A mission design involving spacecraft formation flying can provide numerous operational and financial advantages. For example, under the current sensing and imaging technology, an individual spacecraft is assigned a finite aperture area to retain the satellite's orbit and a larger spacecraft is required to obtain wider regions of coverage. However, launching a large spacecraft so that it escapes the atmosphere requires a large amount of fuel and may even result in total mission loss in the event of a spacecraft subsystem failure. On the other hand, multiple small satellites in formation flight can cover a wider area for sensing and imaging. In addition to coverage of a wider area, the resolution of the imaging sensors in spacecraft formation flight missions may be improved by using multiple sensors. A fleet of collaborating spacecraft can work like a single array, producing a large synthetic aperture that would not be feasible with only a single spacecraft.

In recent years, formation flight control for multiple satellites or vehicles has received much interest. The formation flight controllers that are used in this type of flight control are generally categorized into the centralized type and the decentralized type, which are distinguished based on where the control decisions are made. Centralized control [1] is a type of coordinated control in which a single control agent determines the control actions for the distributed system. Decentralized control [2] is a type of control in which the control decisions are relegated to the local control agents. The local control agents use local observations and/or any information communicated from the other control agents to determine the control actions.

Centralized control has two primary benefits over decentralized control: the formation-keeping performance and the simple formation algorithm. Because the entire system is controlled by the command signal of a leader, the formation can be easily maintained.

Presented as Paper 6471 at the AIAA Guidance, Navigation, and Control Conference, Honolulu, HI, 18–21 August 2008; received 3 July 2008; revision received 16 March 2009; accepted for publication 16 March 2009.

*Graduate Student, School of Mechanical and Aerospace Engineering; sety@snu.ac.kr. Student Member AIAA.

†Professor, School of Mechanical and Aerospace Engineering, Institute of Advanced Aerospace Technology; ydkim@snu.ac.kr. Senior Member AIAA.

In other words, the followers only require the command signal from the leader to keep their formation. Therefore, the system can implement the formation-keeping algorithm simply and easily. However, the centralized control scheme requires much more information and processing time than its counterpart, the decentralized scheme. The failure of the leader in the centralized controlled system may destabilize the entire system. The decentralized control scheme has the advantage of fault tolerance, and its failure is confined to the region of the local control agent that failed, resulting in only a small degradation in system performance. However, the decentralized control scheme also has a drawback, in that its control system is difficult to analyze.

Under the virtual structure approach, which is a type of centralized control, very difficult missions can be executed in both gravity-influenced and deep space environments [3]. The virtual structure approach treats the entire formation as a virtual rigid-body structure [4,5]. This approach maintains the geometric relationships among the spacecraft during a maneuver. Using the virtual structure approach, Hammer et al. [6] and Malla et al. [7] introduced the spacecraft formation flying method, which allows synchronized maneuvers to point the formation in a desired direction. In these previous works, the authors used a simple deep space model. They did not consider the gravity effect and disturbances and simply considered Newton's second law for description of position dynamics, that is, $f_i = M_i V_i$. This simple position dynamics enables the designer to deal with the problem easily. In this study, however, the relative motion of each satellite with respect to the reference Earth orbit is considered. Not only is the gravity effect considered, but also the mass variation of the satellite and external disturbances. And, also in these previous works, the authors used Euler angle transformation to make two vectors point in the same direction. This method requires two transformations. The two transformation matrices of the azimuth and elevation angles must be obtained from the geometric relation between the satellite and virtual structure. The development of such matrices is quite cumbersome work. Therefore, in this study, one transformation matrix is used, which is calculated based on the only required information, that is, the principal axis vector and principal angle of rotation. Therefore, the azimuth and elevation angle of each satellite do not have to be calculated in each step. In there previous works, the formulation flying algorithm only makes the satellites point toward the same direction so that the line-of-sight vector of each satellite is parallel to the others. In this study, the formation flying algorithm can control the attitude of each satellite for one-point targeting. Therefore, the proposed formation flying algorithm enables the satellite system to perform various missions, such as 3-D photographing, energy transfer using microwaves, and missile/asteroid interception using laser equipment.

An adaptive sliding mode control scheme is adopted to make each satellite follow the reference command from the virtual structure algorithm. In past decades, adaptive control and the sliding mode control for nonlinear systems have been studied extensively to achieve robust control performance. In this study, a proper adaptive sliding mode control law to handle a second-order nonlinear system is proposed because second-order nonlinear dynamics can represent the coupled position and attitude dynamics of a satellite. Sliding variables are considered [8] in the design procedure of the adaptive control; therefore, modeling uncertainties and disturbances can be alleviated, and the problems of the sliding mode control scheme can be overcome.

This paper proposes a new systematic formation scheme that will make multiple satellites point toward a single target simultaneously. The design procedure relies on the concept of a virtual structure and coordinate transformation. The proposed formation flying algorithm calculates the necessary rotation angles and translational displacements based on the target and the coordinate of each satellite. This paper also proposes a new robust nonlinear control law, which can make the system track the reference command despite uncertainties and disturbances. The proposed adaptive sliding mode control law can make the system robustly track the formation flying command given by the virtual structure algorithm despite the uncertainties.

II. Spacecraft Dynamics

A 6-degree-of-freedom dynamic model is considered in this study. In this section, the nonlinear model of the relative position dynamics and the attitude dynamics of the satellite will be briefly described.

A. Relative Position Dynamics

In this study, a rotating local-vertical–local-horizontal (LVLH) frame is used to visualize the relative motion of each satellite with respect to the reference satellite. The y axis points in the radial direction, the z axis is perpendicular to the orbital plane and points in the direction of the angular momentum vector, and the x axis points in the opposite-track direction. The relative motion dynamics can be derived using Lagrangian mechanics based on the LVLH frame [9] by using the fact that the total energy of the satellite is conserved under the gravitational field.

In Fig. 1, it is assumed that the inertial coordinate system, $\{X \quad Y \quad Z\}$, is attached to the center of the Earth, and $\Re$ denotes the position vector from the origin of the inertial coordinate frame to the leader spacecraft. A right-hand coordinate frame, $\{x \quad y \quad z\}$, is also attached to the leader spacecraft. The relative dynamics for an eccentric reference orbit can be represented as

$$\ddot{x} = 2\dot{\theta}\dot{y} + \ddot{\theta}y + \theta^2 x - \frac{\mu x}{\|x\hat{\mathbf{i}} + (y+\Re)\hat{\mathbf{j}} + z\hat{\mathbf{k}}\|^3} + \frac{F_x}{m} \tag{1}$$

$$\ddot{y} = -2\dot{\theta}\dot{x} - \ddot{\theta}x + \dot{\theta}^2 y - \mu\left(\frac{y+\Re}{\|x\hat{\mathbf{i}} + (y+\Re)\hat{\mathbf{j}} + z\hat{\mathbf{k}}\|^3} - \frac{\Re}{\|\Re\hat{\mathbf{j}}\|^3}\right) + \frac{F_y}{m} \tag{2}$$

$$\ddot{z} = -\frac{\mu z}{\|x\hat{\mathbf{i}} + (y+\Re)\hat{\mathbf{j}} + z\hat{\mathbf{k}}\|^3} + \frac{F_z}{m} \tag{3}$$

B. Attitude Dynamics in Quaternion Form

The attitude dynamics of a satellite is governed by the following equation [10]:

$$J\dot{\boldsymbol{\omega}}_B = -\tilde{\boldsymbol{\omega}}_B J\boldsymbol{\omega}_B + \boldsymbol{\tau} \tag{4}$$

$$\dot{\mathbf{q}} = -\frac{1}{2}\begin{bmatrix} -\tilde{\boldsymbol{\omega}}_B & \boldsymbol{\omega}_B \\ -\boldsymbol{\omega}_B^T & 0 \end{bmatrix}\mathbf{q} \tag{5}$$

$$\tilde{\boldsymbol{\omega}}_B = \begin{bmatrix} 0 & -\omega_3 & \omega_2 \\ \omega_3 & 0 & -\omega_1 \\ -\omega_2 & \omega_1 & 0 \end{bmatrix} \tag{6}$$

where $J = J(m) \in R^{3\times3}$ is the mass-dependent inertia, $\boldsymbol{\omega}_B \in R^{3\times1}$ is the satellite body angular velocity, and $\boldsymbol{\tau} \in R^{3\times1}$ is the control torque. In quaternion kinematics, $\mathbf{q} \equiv [\mathbf{q}_v^T \quad q_4]^T$ and $\mathbf{q}\cdot\mathbf{q} = 1$, where $\mathbf{q}_v \in$

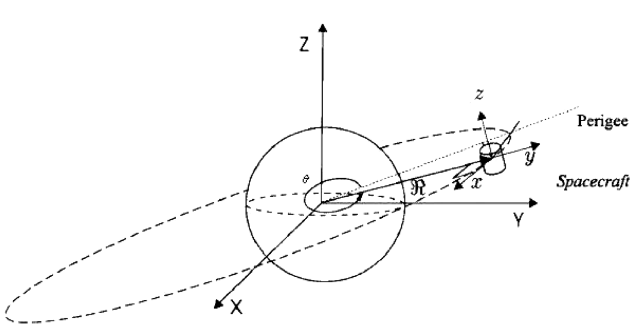

Fig. 1 Schematic representation of the LVLH frame.

$$\mathbf{B}_b = \begin{bmatrix} 0 & 0 & 1 & -1 & 0 & 0 & 0 & 0 & 1 & -1 & 0 & 0 \\ 0 & 0 & 0 & 0 & 1 & -1 & 0 & 0 & 0 & 0 & 1 & -1 \\ 1 & -1 & 0 & 0 & 0 & 0 & 1 & -1 & 0 & 0 & 0 & 0 \\ L_2/2 & L_2/2 & 0 & 0 & L_3/2 & L_3/2 & -L_2/2 & -L_2/2 & 0 & 0 & -L_3/2 & -L_3/2 \\ -L_1/2 & -L_1/2 & L_3/2 & L_3/2 & 0 & 0 & -L_1/2 & -L_1/2 & -L_3/2 & -L_3/2 & 0 & 0 \\ 0 & 0 & -L_2/2 & -L_2/2 & L_1/2 & L_1/2 & 0 & 0 & -L_2/2 & -L_2/2 & L_1/2 & L_1/2 \end{bmatrix} \tag{13}$$

$R^{3\times1}$ is the vector part and q_4 is the scalar part of the quaternion. A vector with a tilde denotes the skew symmetric matrix of this vector, as shown in Eq. (6).

Taking the derivative of Eq. (5) yields

$$\ddot{\mathbf{q}} = \frac{1}{2}\begin{bmatrix} -\dot{\tilde{\boldsymbol{\omega}}}_B & \dot{\boldsymbol{\omega}}_B \\ -\dot{\boldsymbol{\omega}}_B^T & 0 \end{bmatrix}\mathbf{q} + \frac{1}{2}\begin{bmatrix} -\tilde{\boldsymbol{\omega}}_B & \boldsymbol{\omega}_B \\ -\boldsymbol{\omega}_B^T & 0 \end{bmatrix}\dot{\mathbf{q}} \tag{7}$$

Equation (4) can be rewritten as

$$\dot{\boldsymbol{\omega}}_B = J^{-1}[-\tilde{\boldsymbol{\omega}}_B J\boldsymbol{\omega}_B + \boldsymbol{\tau}] \equiv \mathbf{p} + J^{-1}\boldsymbol{\tau} \tag{8}$$

Substitution of Eq. (8) into Eq. (7) gives

$$\ddot{\mathbf{q}} = \frac{1}{2}\begin{bmatrix} -\tilde{\mathbf{p}} & \mathbf{p} \\ -\mathbf{p}^T & 0 \end{bmatrix}\mathbf{q} + \frac{1}{2}\begin{bmatrix} -\tilde{\boldsymbol{\omega}}_B & \boldsymbol{\omega}_B \\ -\boldsymbol{\omega}_B^T & 0 \end{bmatrix}\dot{\mathbf{q}} + \frac{1}{2}\begin{bmatrix} \tilde{\mathbf{q}} + q_4\mathbf{I}_{3\times3} \\ -\mathbf{q}_v^T \end{bmatrix}\mathbf{J}^{-1}\boldsymbol{\tau} \tag{9}$$

Equations (1–3) and (9) form a position and attitude dynamics model of the satellite. Let us define a new state vector $\mathbf{x} \equiv [x \quad y \quad z \quad \mathbf{q}^T]^T$ and a control vector $\underline{\mathbf{u}} \equiv [\mathbf{F}^T \quad \boldsymbol{\tau}^T]^T \in R^{6\times1}$, and then the nonlinear dynamics of Eqs. (1–3) and (9) can be written as

$$\ddot{\mathbf{x}} = \mathbf{f}(\mathbf{x}, \dot{\mathbf{x}}) + \mathbf{B}\underline{\mathbf{u}} \tag{10}$$

where

$$\mathbf{f} \equiv \begin{bmatrix} 2\dot{\theta}\dot{y} + \ddot{\theta}y + \theta^2 x - \mu x/\|x\hat{\mathbf{i}} + (y+\Re)\hat{\mathbf{j}} + z\hat{\mathbf{k}}\|^3 \\ -2\dot{\theta}\dot{x} - \ddot{\theta}x + \dot{\theta}^2 y - \mu(y+\Re/\|x\hat{\mathbf{i}} + (y+\Re)\hat{\mathbf{j}} + z\hat{\mathbf{k}}\|^3 - \Re/\|\Re\hat{\mathbf{j}}\|^3) \\ -\mu z/\|x\hat{\mathbf{i}} + (y+\Re)\hat{\mathbf{j}} + z\hat{\mathbf{k}}\|^3 \\ \frac{1}{2}\begin{bmatrix} -\tilde{\mathbf{p}} & \mathbf{p} \\ -\mathbf{p}^T & 0 \end{bmatrix}\mathbf{q} + \frac{1}{2}\begin{bmatrix} -\tilde{\boldsymbol{\omega}}_B & \boldsymbol{\omega}_B \\ -\boldsymbol{\omega}_B^T & 0 \end{bmatrix}\dot{\mathbf{q}} \end{bmatrix} \tag{11}$$

$$\mathbf{B} \equiv \begin{bmatrix} \frac{\mathbf{I}_{3\times3}}{m} & \mathbf{0}_{3\times3} \\ \mathbf{0}_{4\times3} & \frac{1}{2}\begin{bmatrix} \tilde{\mathbf{q}} + q_4\mathbf{I}_{3\times3} \\ -\mathbf{q}^T \end{bmatrix}\mathbf{J}^{-1} \end{bmatrix} \tag{12}$$

Note that the dimensions of the zero matrices are determined by the number of thrusters and their arrangement.

C. Thruster Layout and System Dynamics

This study assumes that a total of 12 thrusters are used to control the position and attitude of the satellite, as shown in Fig. 2 [10]. The input matrix of the system expressed in the satellite body frame $\mathbf{B}_b$ can be defined as

where L_i is the dimensions of the satellite, as shown in Fig. 2. The maximum value of thrust is assumed to be 0.67 N in this study.

Because thrust forces are expressed in the satellite body frame, they should to be transformed into the LVLH coordinate system. Then, the control input $\underline{\mathbf{u}}$ can be derived as

$$\underline{\mathbf{u}} = \begin{bmatrix} \mathbf{C}_{BL} & \mathbf{0}_{3\times3} \\ \mathbf{0}_{3\times3} & \mathbf{I}_{3\times3} \end{bmatrix}\mathbf{B}_b\mathbf{u}_\mathbf{f} \equiv \mathbf{B}_a\mathbf{B}_b\mathbf{u}_\mathbf{f} \tag{14}$$

where $\mathbf{u}_\mathbf{f} = [\mathbf{f}_1 \quad \mathbf{f}_2 \quad \cdots \quad \mathbf{f}_{12}]^T$ is the thrust force vector, and the coordinate translation matrix C_{BL} is defined using the quaternion of the satellite as

$$\mathbf{C}_{BL} = \begin{bmatrix} 1-2(q_2^2+q_3^2) & 2(q_1q_2+q_3q_4) & 2(q_1q_3-q_2q_4) \\ 2(q_2q_1-q_3q_4) & 1-2(q_1^2+q_3^2) & 2(q_2q_3+q_1q_4) \\ 2(q_3q_1+q_2q_4) & 2(q_3q_2-q_1q_4) & 1-2(q_1^2+q_2^2) \end{bmatrix}^T \tag{15}$$

Finally, the resulting dynamics model of Eq. (10) can be rewritten as follows:

$$\begin{aligned} \ddot{\mathbf{x}} &= \mathbf{f}(\mathbf{x}, \dot{\mathbf{x}}, \mathbf{t}) + \mathbf{B}\underline{\mathbf{u}} = \mathbf{f}(\mathbf{x}, \dot{\mathbf{x}}, \mathbf{t}) + \mathbf{B}\mathbf{B}_a\mathbf{B}_b\mathbf{u}_\mathbf{f} \\ &\equiv \mathbf{f}(\mathbf{x}, \dot{\mathbf{x}}, \mathbf{t}) + \boldsymbol{\Pi}\mathbf{u}_\mathbf{f} \end{aligned} \tag{16}$$

where $\boldsymbol{\Pi} \equiv \mathbf{B}\mathbf{B}_a\mathbf{B}_b$. Note that, for this particular thruster configuration, input matrix $\boldsymbol{\Pi}$ and control input vector $\mathbf{u}_\mathbf{f}$ should be used instead of $\mathbf{B}$ and $\underline{\mathbf{u}}$ for designing the controller and for the numerical simulation.

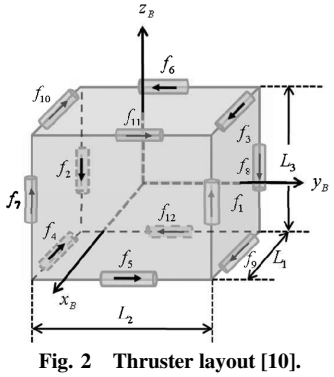

Fig. 2 Thruster layout [10].

III. Virtual Structure Formation Flight Algorithm

In this section, the virtual-structure-based formation control is presented. Assume that the position vectors of three satellites and the position vector of the target are known, and that the camera or laser equipment of the satellite is aligned with the satellite's z axis of the body coordinate system. This paper assumes that there are three satellites. However, this algorithm can be expanded to a larger configuration with more satellites. The objective of this study is to design a single target pointing algorithm for multiple satellites in a desired formation. Figure 3 shows the geometry of the virtual structure model. The three apexes, A, B, and C, represent the first, second, and third satellites with respect to the inertial frame $\{x, y, z\}$, and **T** is the target object in the inertial frame. The formation reference frame for the satellites is placed at the centroid **X** of the virtual structure. Each satellite uses this formation reference frame to track its desired positions with respect to the positions of other satellites during maneuvers.

The virtual structure formation flight algorithm makes the satellites point toward the desired target simultaneously in three stages. The first stage is virtual structuring; in this stage, the virtual structure and vectors required to calculate the reference command signal are defined, and the axis of sight of each satellite is aligned with the bore sight vector of the virtual structure. The second stage is virtual structure rotation; in this stage, the virtual structure is rotated to align its bore sight vector with the target vector. The third stage is the targeting stage; in this stage, each satellite is rotated to point toward the desired target. Detailed procedures of the three stages will be presented in the following sections.

A. First Stage: Virtual Structuring

First, the virtual structure has to be defined using the position vectors of the three satellites. It is assumed that the position vectors of each satellite are known. Then, the centroid vector and the bore sight vector can be defined. The bore sight vector originates from the centroid of the formation triangle and is pointed normal to the two-dimensional plane in which the formation exists. Using the inertial frame, the centroid vector **X** and the bore sight vector **S** can be calculated as

$$\mathbf{X} = \frac{\mathrm{A} + \mathrm{B} + \mathrm{C}}{3} \tag{17}$$

$$\mathbf{S} = \mathbf{X}\mathrm{A} \times \mathbf{X}\mathrm{C} \tag{18}$$

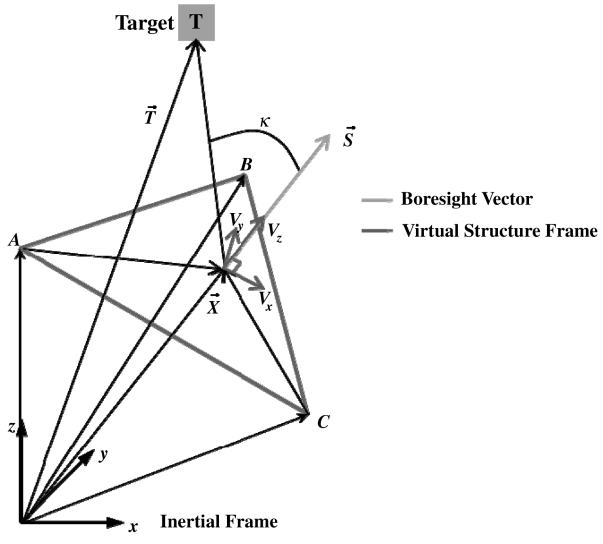

Fig. 3 Virtual structure model in 3-D space.

Let us define the virtual structure frame (VSF), which originates from the centroid of the virtual structure. The z axis of the VSF is the bore sight vector and the y axis is directed toward one particular satellite. The three axes of the VSF can be expressed as follows in the inertial frame:

$$\mathbf{V_z} = \mathbf{S}/|\mathbf{S}| \qquad \mathbf{V_y} = \mathbf{X}\mathrm{B}/|\mathbf{X}\mathrm{B}| \qquad \mathbf{V_x} = \mathbf{V_y} \times \mathbf{V_z} \tag{19}$$

Now, the coordinate transformation matrix R_1 from the inertial frame to the VSF can be obtained as

$$R_1 = [\,\mathbf{V_x} \quad \mathbf{V_y} \quad \mathbf{V_z}\,] \tag{20}$$

The procedure of the virtual structuring stage aligns the attitude of each satellite to the VSF direction. Now, the cosine rule is applied to calculate the maneuver angle κ between the bore sight vector **S** and the vector from the centroid to the target object, **X**T. The maneuver angle, κ, is defined as

$$\kappa = \cos^{-1}\left(\frac{\mathbf{S} \cdot \mathbf{X}\mathrm{T}}{|\mathbf{S}| \cdot |\mathbf{X}\mathrm{T}|}\right) \tag{21}$$

B. Second Stage: Virtual Structure Rotation

In the first stage, the virtual structure rotation is performed to align the bore sight vector **S** with the target vector **X**T. If the principal axis and the principal angle are known, the coordinate transformation matrix from the inertial frame to the desired frame can be obtained using the following equation [11]:

$$R_2 = \begin{bmatrix} l_1^2(1-\cos\kappa)+\cos\kappa & l_1 l_2(1-\cos\kappa)-l_3\sin\kappa & l_1 l_3(1-\cos\kappa)+l_2\sin\kappa \\ l_1 l_2(1-\cos\kappa)+l_3\sin\kappa & l_2^2(1-\cos\kappa)+\cos\kappa & l_2 l_3(1-\cos\kappa)-l_1\sin\kappa \\ l_3 l_1(1-\cos\kappa)-l_2\sin\kappa & l_3 l_2(1-\cos\kappa)+l_1\sin\kappa & l_3^2(1-\cos\kappa)+\cos\kappa \end{bmatrix} \tag{22}$$

where $l = [\,l_1 \quad l_2 \quad l_3\,]^T$ is the principal axis vector, and κ is the principal angle of the rotation. Because the principal axis, l, is normal to the vectors **S** and **X**T, the principal axis vector can be defined as

$$l = \frac{\mathbf{S} \times \mathbf{X}\mathrm{T}}{|\mathbf{S} \times \mathbf{X}\mathrm{T}|} \tag{23}$$

Throughout the virtual structure rotation, each satellite moves to a new position, which can be calculated by using Eq. (22) as

$$\mathrm{A}' = \mathbf{X} + \mathbf{X}\mathrm{A}' = \mathbf{X} + R_2\mathbf{X}\mathrm{A} \tag{24}$$

$$\mathrm{B}' = \mathbf{X} + \mathbf{X}\mathrm{B}' = \mathbf{X} + R_2\mathbf{X}\mathrm{B} \tag{25}$$

$$\mathrm{C}' = \mathbf{X} + \mathbf{X}\mathrm{C}' = \mathbf{X} + R_2\mathbf{X}\mathrm{C} \tag{26}$$

Figure 4 shows the qualitative procedure of the virtual structure rotation. Note that $\mathbf{S}'$ is a boresight vector after rotation, and axis l is normal to both **S** and **X**T in Fig. 4.

C. Third Stage: Targeting

The attitude of each satellite is coincided with the VSF in the first and second stages, as shown in Fig. 5. Figure 5 shows the top and side views of the system after the virtual structure rotation. Let us first consider satellite A. The satellite only needs to rotate at the rotation

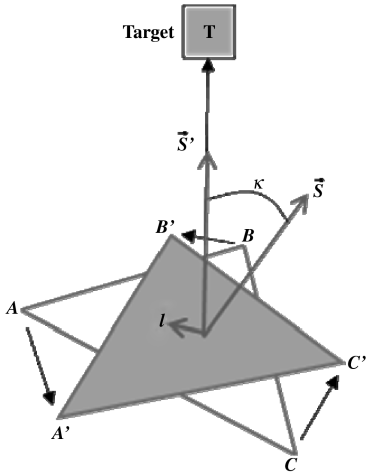

Fig. 4 Virtual structure rotation.

angle γ_A about the new principal axis l_A to point toward the desired target. Because the principal axis l_A is normal to the vectors $\hat{z}_{A'}$ and A**X**, l_A can be determined. Finally, the cosine rule is applied to calculate the principal angle γ_A as

$$l_A = \hat{z}_{A'} \times \frac{A'\mathbf{X}}{|A'\mathbf{X}|} = R_2 R_1 \begin{bmatrix} 0 \\ 0 \\ 1 \end{bmatrix} \times \frac{A'\mathbf{X}}{|A'\mathbf{X}|} \tag{27}$$

$$\gamma_A = \frac{\pi}{2} - \cos^{-1}\left(\frac{A'T \cdot A'\mathbf{X}}{|A'T| \cdot |A'\mathbf{X}|}\right) \tag{28}$$

The rotational matrix of the targeting stage can be obtained by using Eq. (22) because the principal axis and the principal angle of the targeting are known. The only required work is to substitute the principal axis l_A for l and the principal angle γ_A for κ. Therefore, the rotational matrix of the targeting stage of satellite A can be obtained using the following equation:

$$R_A = \begin{bmatrix} l_{A_1}^2(1-\cos\gamma_A) + \cos\gamma_A & l_{A_1}l_{A_2}(1-\cos\gamma_A) - l_{A_3}\sin\gamma_A & l_{A_1}l_{A_3}(1-\cos\gamma_A) + l_{A_2}\sin\gamma_A \\ l_{A_1}l_{A_2}(1-\cos\gamma_A) + l_{A_3}\sin\gamma_A & l_{A_2}^2(1-\cos\gamma_A) + \cos\gamma_A & l_{A_2}l_{A_3}(1-\cos\gamma_A) - l_{A_1}\sin\gamma_A \\ l_{A_3}l_{A_1}(1-\cos\gamma_A) - l_{A_2}\sin\gamma_A & l_{A_3}l_{A_2}(1-\cos\gamma_A) + l_{A_1}\sin\gamma_A & l_{A_3}^2(1-\cos\gamma_A) + \cos\gamma_A \end{bmatrix} \tag{29}$$

where $\hat{l}_A = [\, l_{A_1} \quad l_{A_2} \quad l_{A_3} \,]^T$ is the principal axis of rotation in the targeting stage.

Now, consider satellite B. Because the axis V_y coincides with the y_B axis, the principal axis of targeting is the x_B axis. For the case of satellite C, the principal axis of targeting can be determined by using the geometric relationships between the vectors $\hat{z}_{C'}$ and C**X**. The principal angles of satellites B and C for pointing to the desired target can be obtained in a similar manner to that in the case of satellite A:

$$l_B = x_{B'} = R_2 R_1 [\, 1 \quad 0 \quad 0 \,]^T \tag{30}$$

$$\gamma_B = \frac{\pi}{2} - \cos^{-1}\left(\frac{B'\mathbf{T} \cdot B'\mathbf{X}}{|B'\mathbf{T}| \cdot |B'\mathbf{X}|}\right) \tag{31}$$

$$l_C = z_{C'} \times \frac{C'\mathbf{X}}{|C'\mathbf{X}|} = R_2 R_1 \begin{bmatrix} 0 \\ 0 \\ 1 \end{bmatrix} \times \frac{C'\mathbf{X}}{|C'\mathbf{X}|} \tag{32}$$

$$\gamma_C = \frac{\pi}{2} - \cos^{-1}\left(\frac{C'\mathbf{T} \cdot C'\mathbf{X}}{|C'\mathbf{T}| \cdot |C'\mathbf{X}|}\right) \tag{33}$$

Each satellite can point to a desired target directly throughout the three stages of virtual structure formation flight. The coordinate transformation matrix from the inertial frame to the satellite body frame of the final attitude state can be summarized as follows:

$$C_A = R_A R_2 R_1 \tag{34}$$

$$C_B = R_B R_2 R_1 \tag{35}$$

$$C_C = R_C R_2 R_1 \tag{36}$$

where C_A, C_B, and C_C are the coordinate transformation matrices of satellites A, B, and C, respectively.

Using the coordinate transformation matrix, the desired reference command signal sent to the satellite to point to the target can be obtained by using the following equation [11]:

$$\begin{aligned} q_{1d} &= (C_{23} - C_{32})/4q_4 \qquad q_{2d} = (C_{31} - C_{13})/4q_4 \\ q_{3d} &= (C_{12} - C_{21})/4q_4 \qquad q_{4d} = \sqrt{C_{11} + C_{22} + C_{33} + 1}/2 \end{aligned} \tag{37}$$

where C_{ij} is the (i, j) element of the coordinate transformation matrix C.

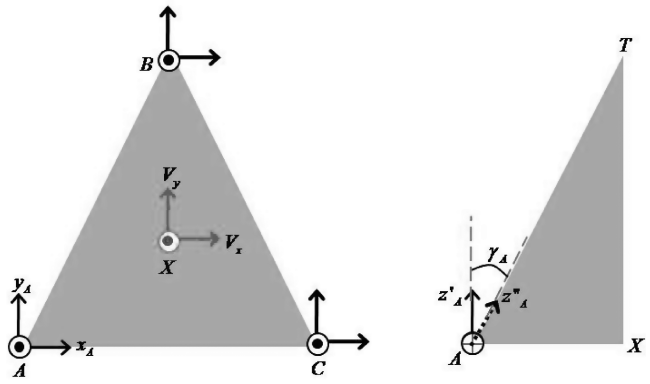

Fig. 5 Top and side view of the system after the virtual structure rotation.

IV. Controller Design

An adaptive control technique is a type of nonlinear feedback control method and is a systematic and recursive design methodology [12]. The adaptive method has characteristics that can accommodate uncertainties and nonlinearities and can avoid wasteful cancellations. On the other hand, trajectories are forced to reach a sliding manifold in finite time in the sliding mode control state and they have to stay on the manifold for all future time. The motion on the manifold is independent of the matched uncertainties. By using a lower-order model, the sliding manifold can be designed to achieve the control objective [13]. The main advantage of the sliding mode controller is that it can achieve the robust stability of the closed-loop system with respect to the model uncertainties,

disturbances, and nonlinear effects. However, pure sliding mode control has some drawbacks, such as large control authority requirements and chattering.

In this study, sliding variables can be considered [8] in the design procedure of adaptive control. By combining the adaptive technique and the sliding mode control scheme, the advantages of both control schemes can be obtained: 1) alleviation of the effects of the modeling uncertainties and disturbances, and 2) resolution of the problems of the sliding mode control scheme such as large control authority requirements.

In this section, an adaptive sliding mode control law is designed for tracking the command signal. Robust tracking performance is obtained by using the proposed control scheme. The theory of the proposed control scheme is derived in the following section, and numerical simulations are performed to demonstrate the effectiveness of the proposed control scheme.

A. Adaptive Sliding Mode Control System

Consider a nonlinear system with both parameter variations and external disturbance. Equation (16) can then be rewritten as

$$\ddot{\mathbf{x}} = [\mathbf{f}(\mathbf{x}, \dot{\mathbf{x}}) + \Delta\mathbf{f}] + [\mathbf{\Pi} + \Delta\mathbf{\Pi}]\mathbf{u_f} + \varsigma \tag{38}$$

where $\Delta\mathbf{f}$ and $\Delta\mathbf{\Pi}$ are the uncertainties introduced by the system parameters, and ς denotes an external disturbance. Equation (38) can be rewritten as

$$\ddot{\mathbf{x}} = [\mathbf{f}(\mathbf{x}, \dot{\mathbf{x}}) + \mathbf{\Pi}\mathbf{u_f} + \upsilon \tag{39}$$

where υ denotes a lumped uncertainty, which is defined as

$$\upsilon = \Delta\mathbf{f} + \Delta\mathbf{\Pi}\mathbf{u_f} + \varsigma \tag{40}$$

The following assumptions are used to design the adaptive controller:

Assumption 1: The desired trajectories $\mathbf{x}_d$ are bounded as

$$\|\mathbf{x}_d\| \le c_d \tag{41}$$

where $c_d \in R$ is a known positive constant, and $\|\cdot\|$ denotes the 2-norm of a vector or a matrix.

Assumption 2: The lumped uncertainty υ is a constant or enough of a slowly varying parameter to approximate $\dot{\upsilon} \approx 0$ during the operation.

Assumption 3: The lumped uncertainty is bounded as

$$|\upsilon| \le \bar{\upsilon} \tag{42}$$

where $\bar{\upsilon} \in R$ is a known positive constant, and $|\cdot|$ denotes the 1-norm of a vector or a matrix.

Assumption 1 means that a physically feasible reference input can be given to the system. By using Assumption 1, a proper command filter can be designed. Assumption 2 will be used in the procedure to derive the adaptive rule for uncertainty estimation, and Assumption 3 will be used in the stability analysis process.

An adaptive sliding mode controller is designed in this study so that the state $\mathbf{x}$ of the system in Eq. (39) can track the reference trajectory $\mathbf{x}_d$. That is, the objective of the adaptive sliding mode control system is to simultaneously achieve relative position and attitude tracking.

Let us introduce the error state variables for tracking as

$$\mathbf{z}_1 = \mathbf{x} - \mathbf{x}_d \tag{43}$$

$$\mathbf{z}_2 = c_1\mathbf{z}_1 + \dot{\mathbf{z}}_1 \tag{44}$$

where c_1 is a positive constant. The dynamic equation of the error state $\mathbf{z}_1$ is given by

$$\dot{\mathbf{z}}_1 = \mathbf{z}_2 - c_1\mathbf{z}_1 \tag{45}$$

The Lyapunov candidate function is chosen as

$$V_1 = \tfrac{1}{2}\mathbf{z}_1^T\mathbf{z}_1 \tag{46}$$

Then, the time derivative of Eq. (46) can be obtained as

$$\dot{V}_1 = \mathbf{z}_1^T\dot{\mathbf{z}}_1 = \mathbf{z}_1^T\mathbf{z}_2 - c_1\mathbf{z}_1^T\mathbf{z}_1 \tag{47}$$

The derivative of $\mathbf{z}_2$ is expressed as

$$\dot{\mathbf{z}}_2 = \tfrac{\mathrm{d}}{\mathrm{d}t}(c_1\mathbf{z}_1 + \dot{\mathbf{z}}_1) = c_1(\mathbf{z}_2 - c_1\mathbf{z}_1) + \mathbf{f} + \mathbf{\Pi}\mathbf{u_f} + \upsilon - \ddot{\mathbf{x}}_d \tag{48}$$

Now, let us define the Lyapunov candidate function with the sliding surface S as

$$V_2 = V_1 + \tfrac{1}{2}S^TS \tag{49}$$

$$S = k_1\mathbf{z}_1 + \mathbf{z}_2 \tag{50}$$

where $k_1 \in R$ is a positive constant. Using Eqs. (47) and (48), the derivative of V_2 can be derived as

$$\dot{V}_2 = \dot{V}_1 + S^TS = \mathbf{z}_1^T\mathbf{z}_2 - c_1\mathbf{z}_1^T\mathbf{z}_1 + S^T(k_1\dot{\mathbf{z}}_1 + \dot{\mathbf{z}}_2) = \mathbf{z}_1^T\mathbf{z}_2 - c_1\mathbf{z}_1^T\mathbf{z}_1 + S^T[(k_1 + c_1)\dot{\mathbf{z}}_1 + \mathbf{f} + \mathbf{\Pi}\mathbf{u_f} + \upsilon - \ddot{\mathbf{x}}_d] \tag{51}$$

The upper bound $\bar{\upsilon}$ is difficult to determine because the lumped uncertainty υ is unknown in the real situation. Therefore, an adaptive law is proposed to adaptively update the value of the lumped uncertainty $\widehat{\upsilon}$. A new Lyapunov candidate function is chosen as

$$V_3 = V_2 + \tfrac{1}{2}\tilde{\upsilon}^T\Gamma^{-1}\tilde{\upsilon} \tag{52}$$

where $\tilde{\upsilon} = \upsilon - \widehat{\upsilon}$, and Γ is a positive definite constant matrix. Differentiating Eq. (52) with respect to time and using Eq. (51), we obtain

$$\dot{V}_3 = \mathbf{z}_1^T\mathbf{z}_2 - c_1\mathbf{z}_1^T\mathbf{z}_1 + S^T[(k_1 + c_1)\dot{\mathbf{z}}_1 + \mathbf{f} + \mathbf{\Pi}\mathbf{u_f} + \widehat{\upsilon} - \ddot{\mathbf{x}}_d] - \tilde{\upsilon}[\Gamma^{-1}\dot{\widehat{\upsilon}} - S] \tag{53}$$

Note that Assumption 2 is used to derive the Eq. (53).

Using Eq. (53), an adaptive sliding mode control law can be proposed as

$$\mathbf{u_f} = \mathbf{\Pi}^{\dagger}[-(k_1 + c_1)\dot{\mathbf{z}}_1 - \mathbf{f} - \widehat{\upsilon} + \ddot{\mathbf{x}}_d - hS - h\beta\mathrm{sgn}(S)] \tag{54}$$

where $S = [S_1 \quad S_2 \quad \cdots \quad S_n]^T \in R^n$ with $n = \dim(\mathbf{x})$, $\mathrm{sgn}(S) = [\mathrm{sgn}(S_1) \quad \mathrm{sgn}(S_2) \quad \cdots \quad \mathrm{sgn}(S_n)]^T$, and h and β are positive constants. Note that $(\cdot)^{\dagger}$ denotes a pseudoinverse; therefore, a minimum norm solution is obtained. The adaptive law for $\dot{\widehat{\upsilon}}$ can be designed as

$$\dot{\widehat{\upsilon}} = \Gamma S \tag{55}$$

Substituting Eqs. (54) and (55) into Eq. (53), the following equation can be obtained:

$$\dot{V}_3 = \mathbf{z}_1^T\mathbf{z}_2 - c_1\mathbf{z}_1^T\mathbf{z}_1 - h\|S\|^2 - h\beta\sum_{i=1}^{n}|S_i| = \mathbf{z}_1^T\mathbf{z}_2 - c_1\mathbf{z}_1^T\mathbf{z}_1 - h\|k_1\mathbf{z}_1 + \mathbf{z}_2\|^2 - h\beta\sum_{i=1}^{n}|S_i| \tag{56}$$

Equation (56) can then be rewritten as

$$\dot{V}_3 = -\mathbf{Z}^TQ\mathbf{Z} - h\beta\sum_{i=1}^{n}|S_i| \tag{57}$$

where

$$Q = \begin{bmatrix} c_1 + hk_1^2 & hk_1 - 1/2 \\ hk_1 - 1/2 & h \end{bmatrix} \tag{58}$$

$$\mathbf{Z}^T = [\,\mathbf{z}_1^T \quad \mathbf{z}_2^T\,] \tag{59}$$

Note that a sufficient condition for the positive definite matrix Q is

$$|Q| = h(c_1 + hk_1^2) - (hk_1 - 1/2)^2 = h(c_1 + k_1) - 1/4 > 0 \tag{60}$$

This condition can be satisfied by proper selection of c_1, k_1, and h.

B. Stability Analysis

The following theorem is considered for the stability analysis of the proposed control law.

Theorem 1: Consider a system in Eq. (39) with the control input of Eq. (54) and the adaptive law of Eq. (55). The state $\mathbf{x}$ then converges to $\mathbf{x}_d$ as $t \to \infty$ with Assumptions 1–3.

Proof: A Lyapunov candidate function of Eq. (52) is chosen to analyze the stability of the proposed control law. By taking the time derivative of Eq. (52) and substituting Eqs. (54), (55), (58), and (59) into the resulting equation, we obtain Eq. (57). Here, let us define $W(t)$ as

$$W(t) \equiv \varepsilon\left(\mathbf{Z}^T Q\mathbf{Z} + h\beta \sum_{i=1}^{n} |S_i|\right) \le -\dot{V}_3 \tag{61}$$

where $0 < \varepsilon < 1$. From Eq. (61), we have

$$\int_0^t W(t)\,\mathrm{d}\tau \le V_3(0) - V_3(t) \tag{62}$$

Because $V_3(0)$ is bounded and $V_3(t)$ is nonincreasing and bounded, the following result can be obtained:

$$\lim_{t\to\infty} \int_0^t W(t)\,\mathrm{d}\tau \le \infty \tag{63}$$

Also, by Lemma 1, $\dot{W}(t)$ is bounded. Therefore, $W(t)$ is uniformly continuous. Using Barbalat's lemma [14], the following result can be obtained:

$$\lim_{t\to\infty} W(t) = 0 \tag{64}$$

That is, $\mathbf{z}_1$ and $\mathbf{z}_2$ converge to zero as $t \to \infty$. It can then be concluded that $\lim_{t\to\infty}(\mathbf{x} - \mathbf{x}_d) = 0$. As a result, the stability and tracking performance of the closed-loop system using the control law of Eq. (54) can be guaranteed. □

Lemma 1: Consider a system in Eq. (39) with the control input of Eq. (54) and the adaptive law of Eq. (55). Then, time derivative of Eq. (61), that is $\dot{W}(t)$, is bounded.

Proof: By the Lyapunov candidate function of Eq. (52) and its time derivative of Eq. (57), the following result can be obtained:

$$V_3 = \tfrac{1}{2}\mathbf{z}_1^T\mathbf{z}_1 + \tfrac{1}{2}S^T S + \tfrac{1}{2}\tilde{\upsilon}^T\Gamma^{-1}\tilde{\upsilon} \ge 0 \tag{65}$$

$$\dot{V}_3 = -\mathbf{Z}^T Q\mathbf{Z} - h\beta\sum_{i=1}^{n}|S_i| \le 0 \tag{66}$$

Equations (65) and (66) imply that $V_3(t) \le V_3(0)$; therefore, $\mathbf{Z}^T = [\,\mathbf{z}_1^T \quad \mathbf{z}_2^T\,]$, S, and $\tilde{\upsilon}$ are bounded. Because $W(t) = \varepsilon(\mathbf{Z}^T Q\mathbf{Z} + h\beta\sum_{i=1}^{n}|S_i|)$ and $\mathbf{u_f} = \mathbf{\Pi}^{\dagger}[-(k_1 + c_1)\dot{\mathbf{z}}_1 - \mathbf{f} - \hat{\upsilon} + \ddot{\mathbf{x}}_d - hS - h\beta\mathrm{sgn}(S)]$, $\dot{W}$ can be written as follows.

Case I: $S = \mathbf{0}$

$$\begin{aligned}\dot{W}(t) &= \varepsilon\frac{\mathrm{d}}{\mathrm{d}t}(\mathbf{Z}^T Q\mathbf{Z}) = \varepsilon(2\mathbf{Z}^T Q\dot{\mathbf{Z}}) \\ &= \varepsilon\left(2\mathbf{Z}^T Q\begin{bmatrix}\mathbf{z}_2 - c_1\mathbf{z}_1 \\ -k_1(\mathbf{z}_2 - c_1\mathbf{z}_1) + \tilde{\upsilon}\end{bmatrix}\right)\end{aligned} \tag{67}$$

Case II: $S_k > 0$, where k is an index such that $|S_k| = \max_i\{|S_1|, |S_2|, \ldots, |S_n|\}$.

Because $\sum_{i=1}^{n}|S_i| \le n\max_i|S_i|$, the following inequality can be concluded:

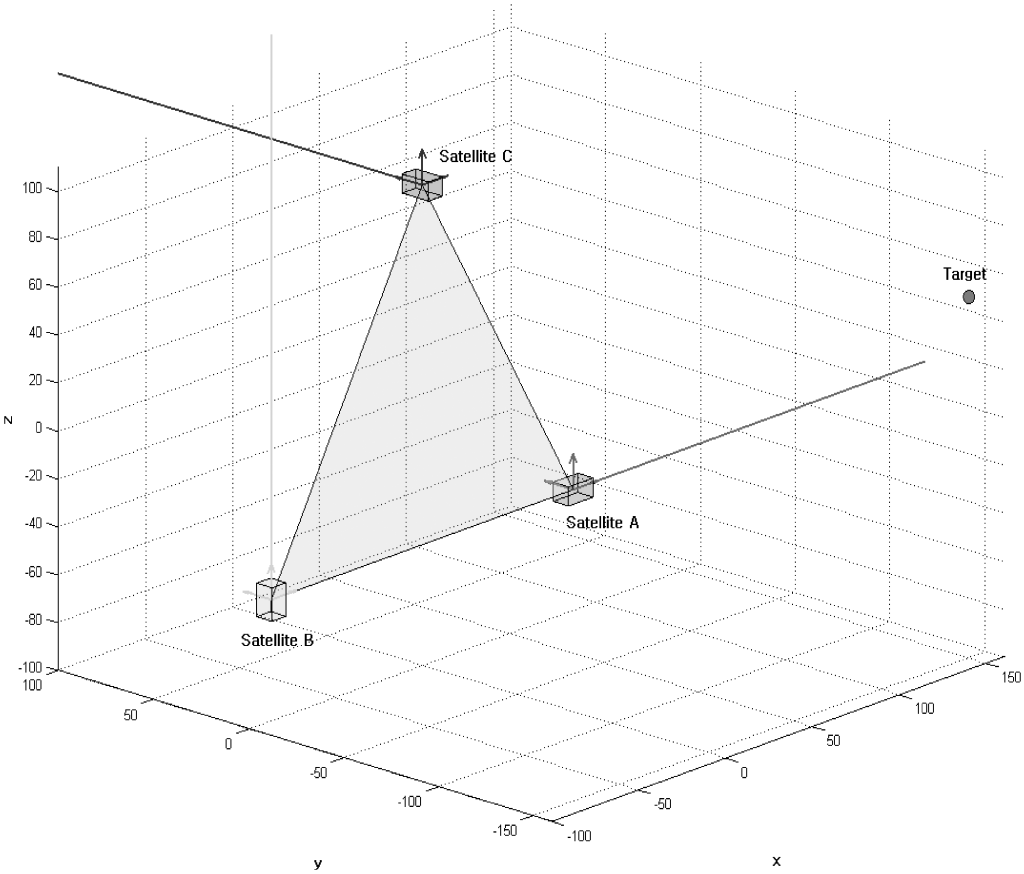

Fig. 6 Initial status of satellites and target, in meters.

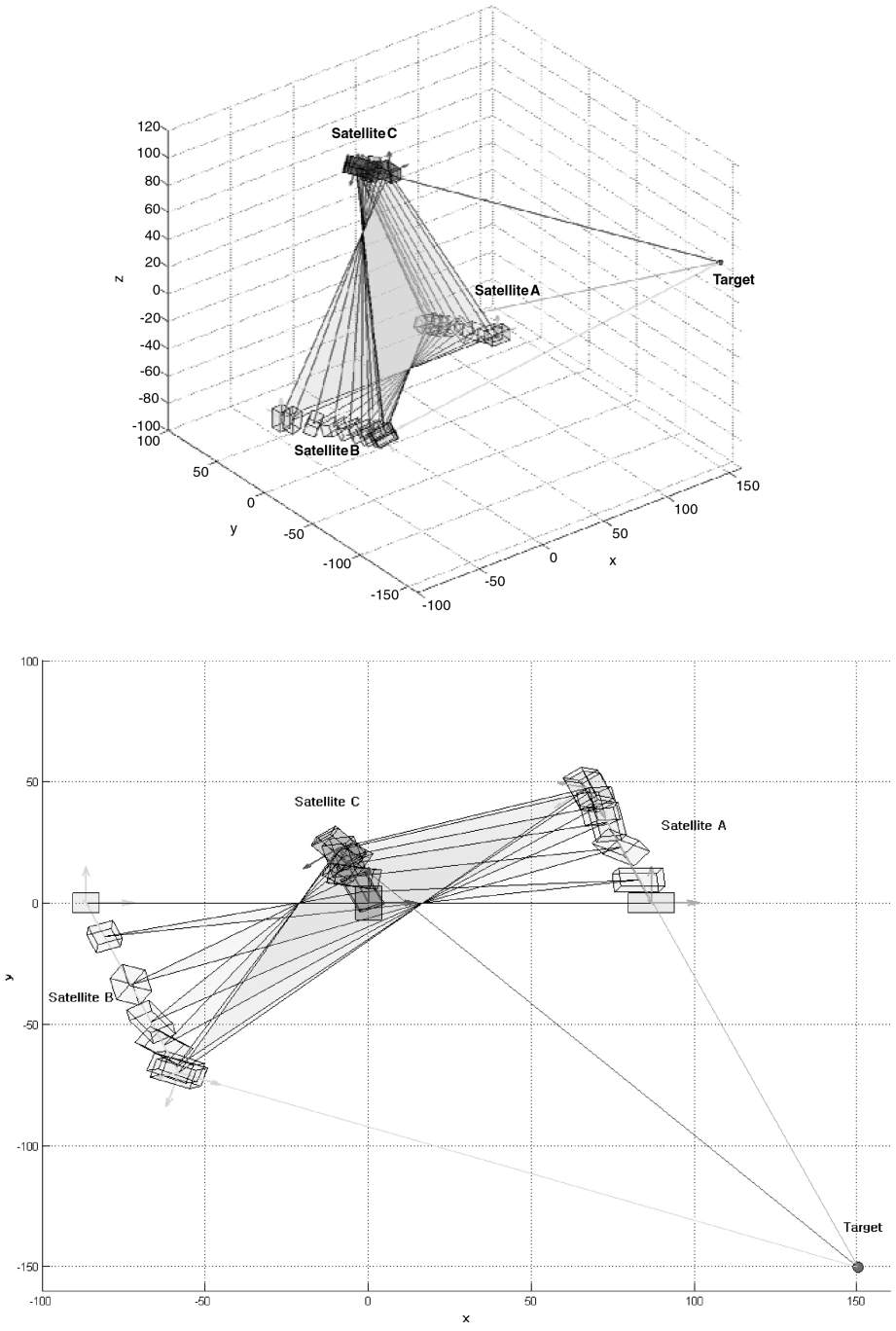

Fig. 7 Position trajectories of each satellite, in meters.

$$\dot{W}(t) = \varepsilon \frac{\mathrm{d}}{\mathrm{d}t}\left(\mathbf{Z}^T Q \mathbf{Z} + h\beta \sum_{i=1}^{n} |S_i|\right)$$
$$\leq \varepsilon \frac{\mathrm{d}}{\mathrm{d}t}(\mathbf{Z}^T Q \mathbf{Z} + h\beta n \max_i |S_i|) = \varepsilon(2\mathbf{Z}^T Q \dot{\mathbf{Z}} + h\beta n \dot{S}_i|_{i=k})$$
$$= \varepsilon\left(2\mathbf{Z}^T Q \begin{bmatrix} \mathbf{z}_2 - c_1 \mathbf{z}_1 \\ -k_1(\mathbf{z}_2 - c_1 \mathbf{z}_1) + \tilde{\upsilon} - hS - h\beta \mathrm{sgn}(S) \end{bmatrix} + h\beta n(\tilde{\upsilon}_k - hS_k - h\beta)\right) \tag{68}$$

Case III: $S_k < 0$ where k is an index such that $|S_k| = \max_i\{|S_1|, |S_2|, \ldots, |S_n|\}$.

Because $\sum_{i=1}^{n} |S_i| \leq n \max_i |S_i|$, the following inequality can be concluded:

$$\dot{W}(t) = \varepsilon \frac{\mathrm{d}}{\mathrm{d}t}\left(\mathbf{Z}^T Q \mathbf{Z} + h\beta \sum_{i=1}^{n} |S_i|\right)$$
$$\leq \varepsilon \frac{\mathrm{d}}{\mathrm{d}t}(\mathbf{Z}^T Q \mathbf{Z} + h\beta n \max_i |S_i|) = \varepsilon(2\mathbf{Z}^T Q \dot{\mathbf{Z}} - h\beta n \dot{S}_i|_{i=k})$$
$$= \varepsilon\left(2\mathbf{Z}^T Q \begin{bmatrix} \mathbf{z}_2 - c_1 \mathbf{z}_1 \\ -k_1(\mathbf{z}_2 - c_1 \mathbf{z}_1) + \tilde{\upsilon} - hS - h\beta \mathrm{sgn}(S) \end{bmatrix} - h\beta n(\tilde{\upsilon}_k - hS_k + h\beta)\right) \tag{69}$$

where $\tilde{\upsilon}_k$ is the kth element of $\tilde{\upsilon}$.

Equations (67–69) show that $\dot{W}$ is bounded, because $\mathbf{Z}$, S, and $\tilde{\upsilon}$ are bounded, as shown in the previous section. □

The convergence of the online estimate vector needs to be analyzed, and the stability analysis of the proposed control law needs to be carried out. The following lemma is used to show the

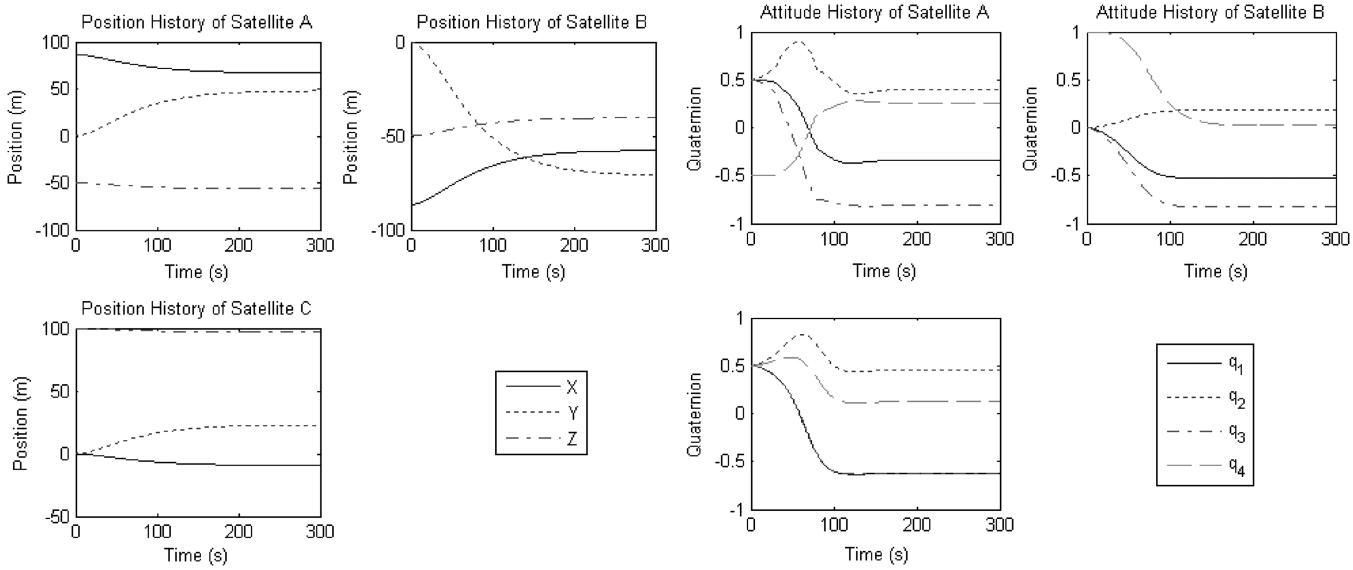

Fig. 8 Position and attitude histories of each satellite.

convergence of the estimated uncertainty vector 16. The result of Lemma 2 is a special case of a general result given by Babalat's lemma.

Lemma 2: If $\varphi, \dot{\varphi} \in \mathcal{L}_\infty$, and $\varphi \in \mathcal{L}_p$ for some $p \in [1, \infty)$, then $\varphi \to 0$ as $t \to \infty$.

The convergence of the online estimated vector is guaranteed with Lemma 2. The analysis process is stated in the following theorem.

Theorem 2: Consider a system of Eq. (39) with the control input of Eq. (54) and the adaptive law of Eq. (55). The estimation error $\tilde{\upsilon}$ then converges to 0 as $t \to \infty$ with Assumptions 1–3.

Proof: Because $V_3 \in \mathcal{L}_\infty$, it can be concluded that $\mathbf{z}_1$, S, and $\tilde{\upsilon} \in \mathcal{L}_\infty$. Using Eq. (55), the following equation can be obtained:

$$\tilde{\upsilon} = \upsilon - \tilde{\upsilon} = \upsilon - \int_0^t \Gamma S \, \mathrm{d}\tau \tag{70}$$

By Assumption 3, we have $\upsilon \in \mathcal{L}_1$. Integrating $W(t)$ in Eq. (62) yields $S \in \mathcal{L}_1$; therefore, $\tilde{\upsilon} \in \mathcal{L}_1$. By Lemma 1, it can be concluded that the estimation error $\tilde{\upsilon} \to 0$ as $t \to \infty$. □

Theorems 1 and 2 demonstrate that both the tracking error and the parameter estimation error of the closed-loop system will converge to zero.

V. Numerical Simulation

A numerical simulation is performed to evaluate the performance of the proposed formation flight controller. The formation under consideration consists of three 40 kg spacecraft flying 100 m apart in an equilateral triangle arrangement in a circular orbit. The gravitational coefficient is $\mu = 3.986 \times 10^{14}$ m^3/s^2, and the orbit radius of the reference satellite is $\Re = 7200$ km. Note that, for a circular orbit, $\dot{\theta} =$ constant and $\ddot{\theta} = 0$. The size of each satellite is assumed to be $0.4 \times 0.1 \times 0.6$ m^3.

The relative position of each satellite and the desired target are initially set as

$$\mathrm{A} = 50\begin{bmatrix} \sqrt{3} \\ 0 \\ -1 \end{bmatrix}, \qquad \mathrm{B} = 50\begin{bmatrix} -\sqrt{3} \\ 0 \\ -1 \end{bmatrix}, \qquad \mathrm{C} = \begin{bmatrix} 0 \\ 0 \\ 10^2 \end{bmatrix}$$

$$\mathrm{T} = 10^2\begin{bmatrix} 1.5 \\ -1.5 \\ 0.5 \end{bmatrix} \tag{71}$$

The origin of the virtual structure frame is located at the center of the

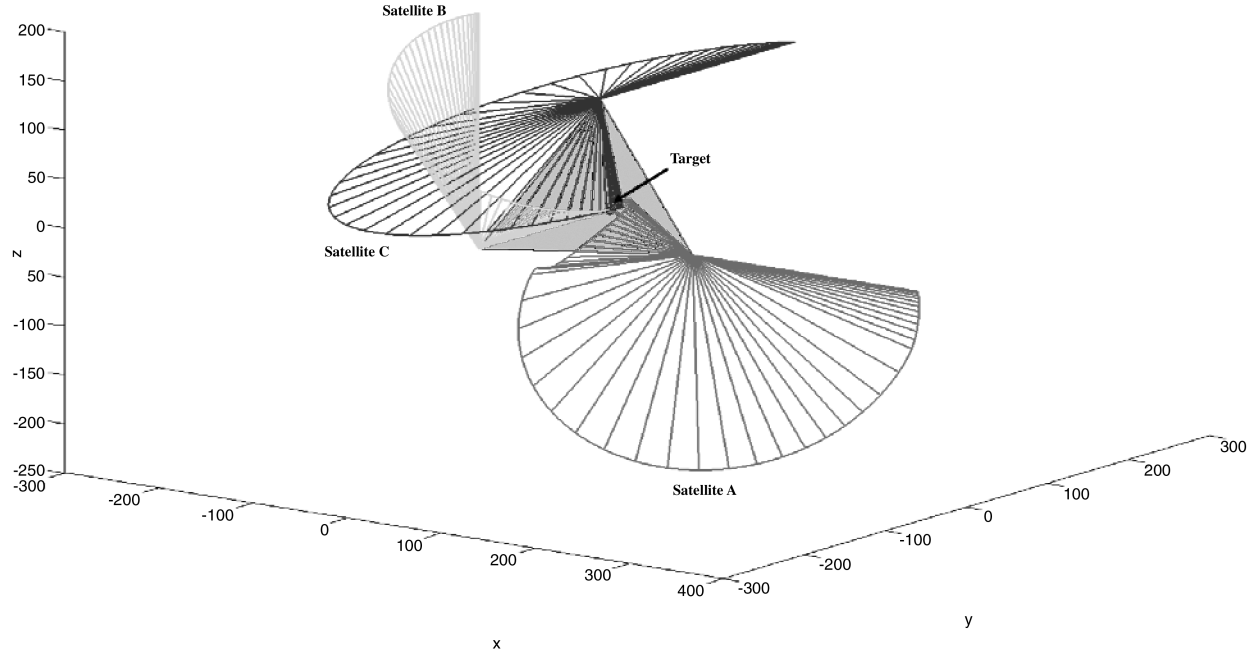

Fig. 9 Three-dimensional trajectories of sight vectors of each satellite relative to the virtual structure, in meters.

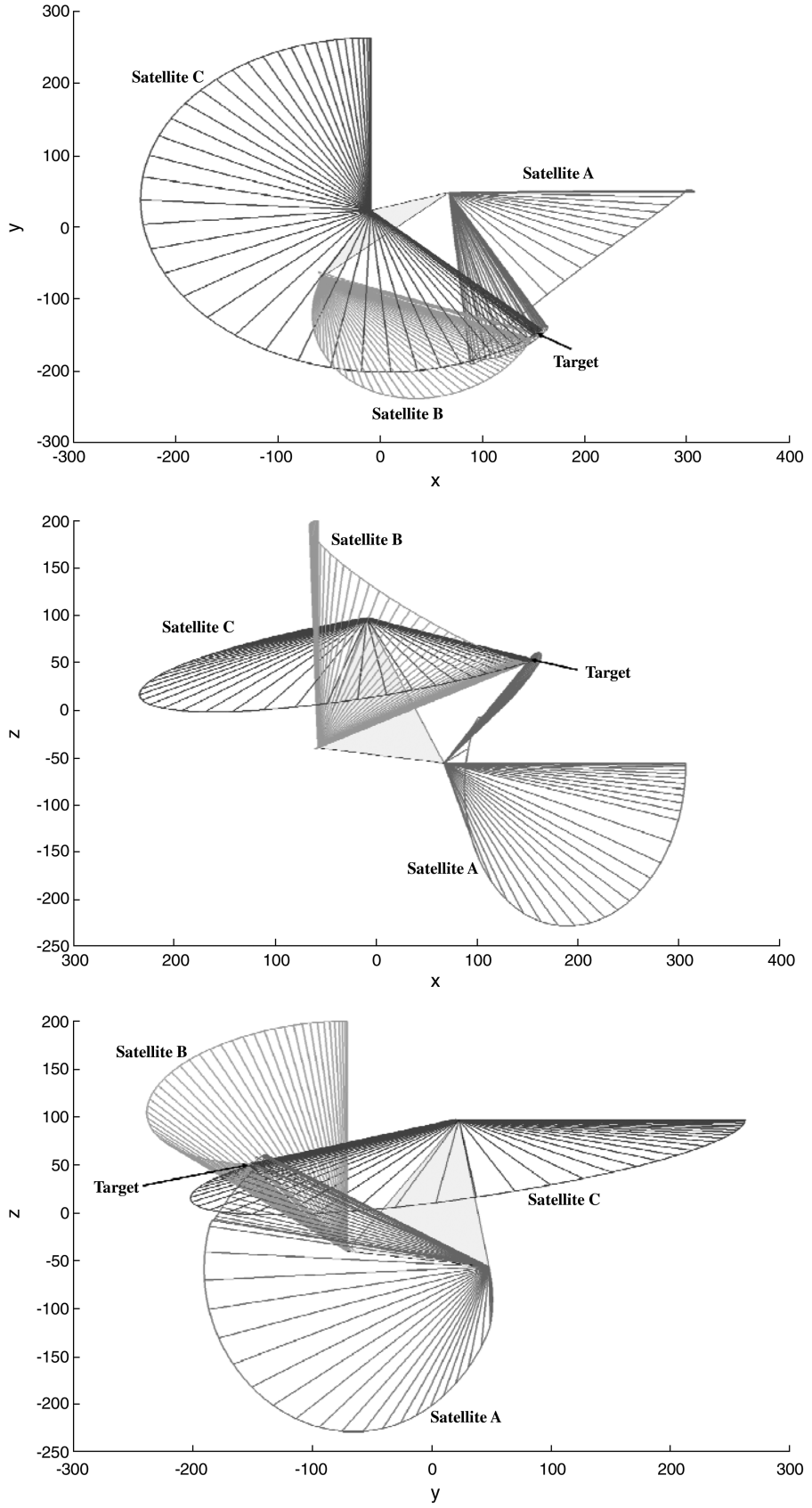

Fig. 10 Projected views of the trajectories of the sight vectors of each satellite, in meters.

triangle, as shown in Fig. 6. The formation bore sight vector is defined to be normal to the spacecraft plane and is therefore initially pointing along the negative y axis.

The mass variation of the satellite due to fuel consumption and the unknown constant external force and torque were considered as the uncertainties. Let us consider N_2H_2 as a propellant. The specific impulse, or I_{sp}, is 320 s. The maximum thrust of the engine is assumed to be 0.67 N. The mass variation of the satellite due to fuel consumption and the unknown constant external translational force and torque disturbances are considered as follows:

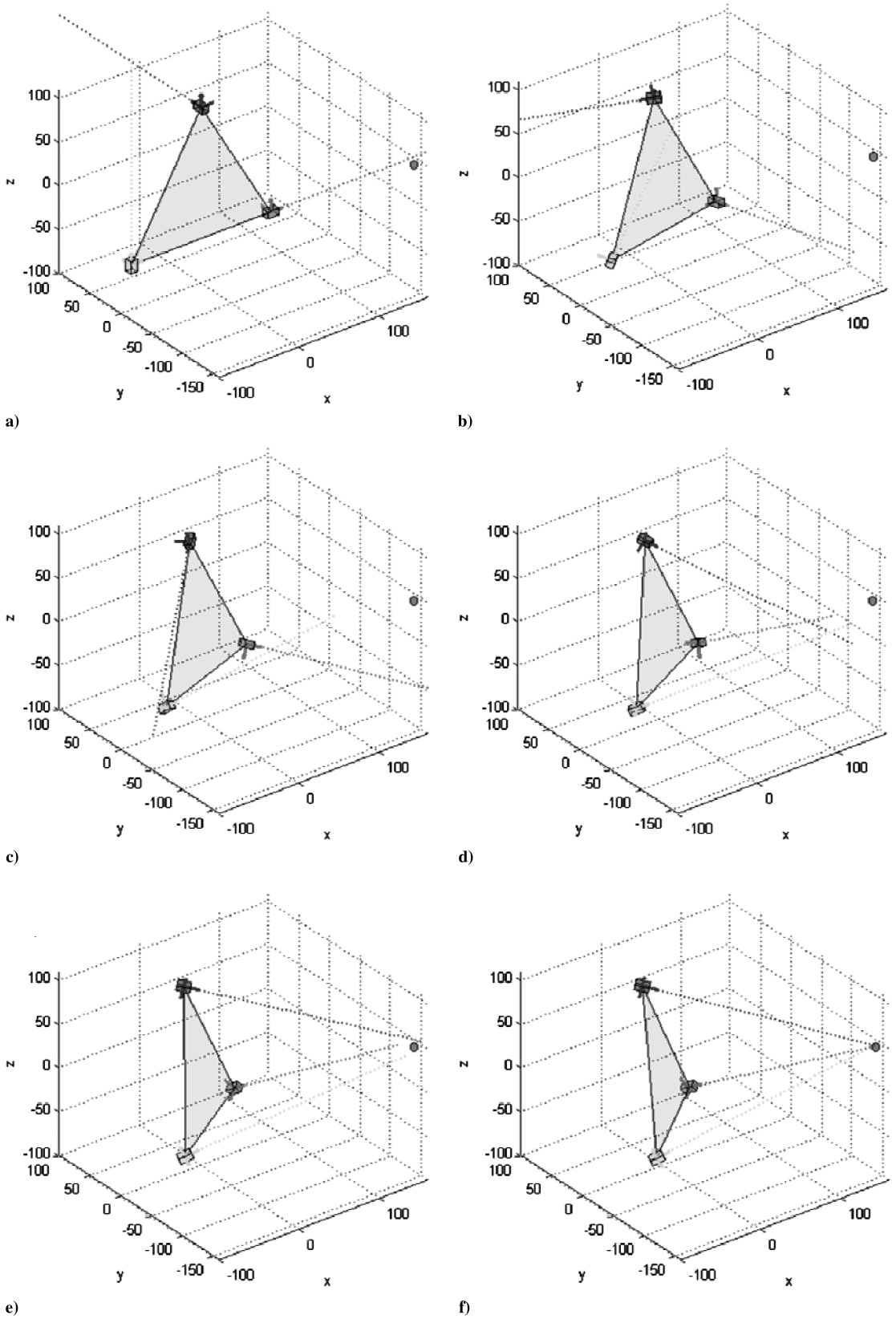

Fig. 11 Changes in position and attitude of each satellite, in meters.

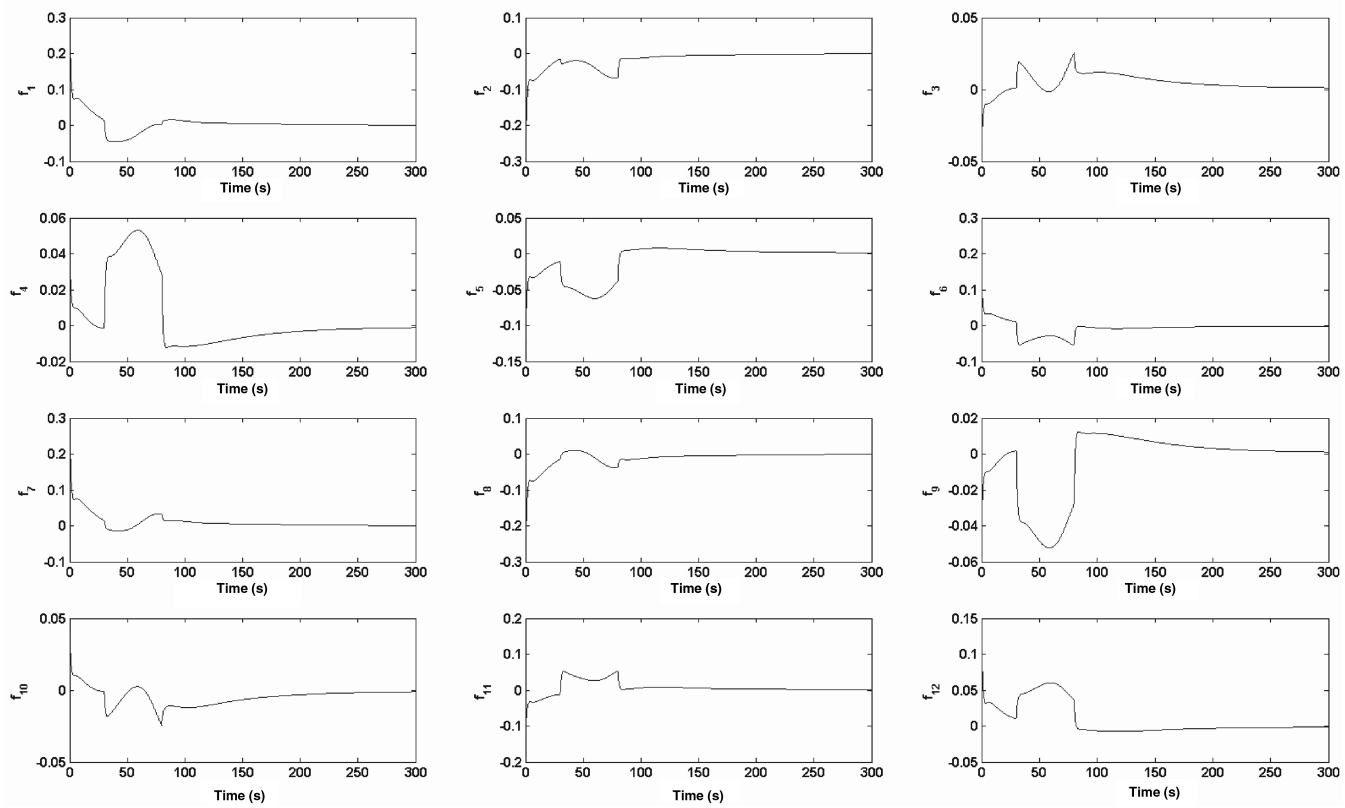

Fig. 12 Thrust inputs of satellite A, in newtons.

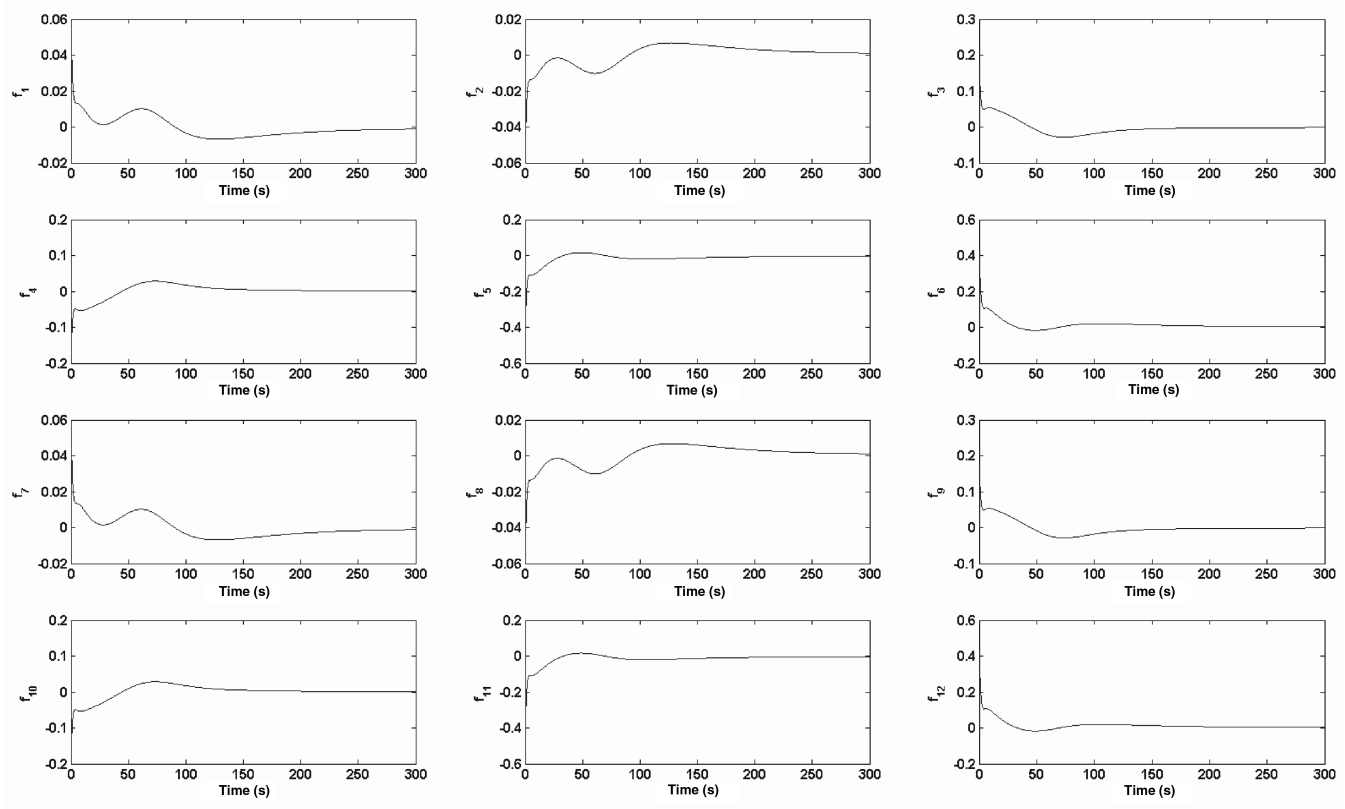

Fig. 13 Thrust inputs of satellite B, in newtons.

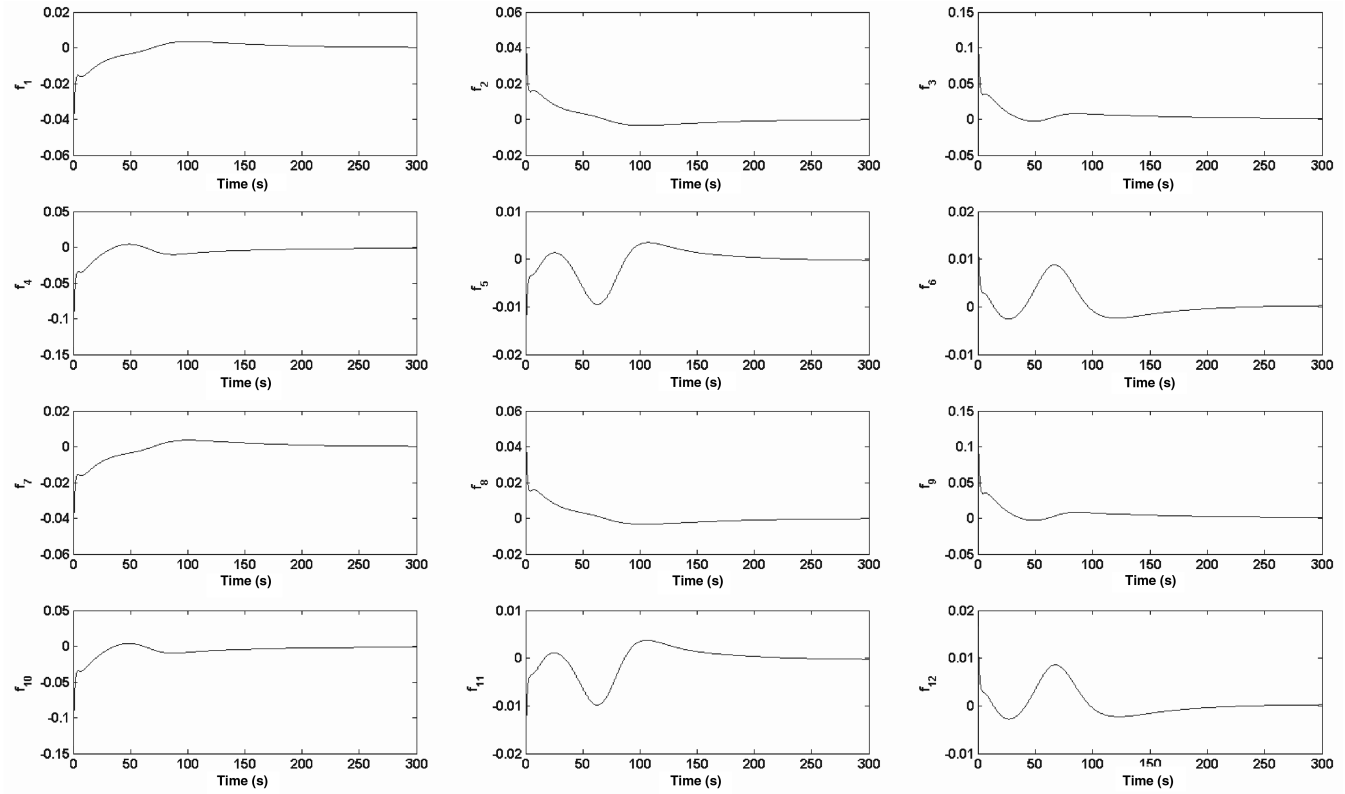

Fig. 14 Thrust inputs of satellite C, in newtons.

$$\dot{m} = -\frac{\sum |u_i|}{I_{\text{sp}} \cdot G} \tag{72}$$

where $G = \mu/R^2$. The specific impulse represents the impulse per unit of propellant. When the propellant with a higher specific impulse is used, the lesser propellant is required to provide a given amount of momentum. An unknown constant disturbance, ς, is considered in the numerical simulation. The values of ς are selected arbitrarily. Note that unknown disturbance is applied to only satellite A.

$$\varsigma = \begin{cases} [-0.0019 \quad 0.0011 \quad 0.0004 \quad -0.03 \quad -0.0225 \quad -0.001 \quad 0.01]^T, & \text{for } 30 \le t \le 80 \\ \mathbf{0}, & \text{otherwise} \end{cases} \tag{73}$$

The proposed formation flight control scheme is applied to the aforementioned mission. Figures 7–11 show the time histories of the position and attitude of each satellite. Figure 7 shows the trajectories of each satellite, which were the result of the first and second stages, that is, virtual structuring and virtual structure rotation. Figure 8 shows the position and attitude histories of each satellite. Each satellite moves to the desired position for construction of the virtual structure and simultaneously rotates to make the bore sight vector of the virtual structure align with the target vector. In the attitude histories of satellite A, a fluctuation due to the unknown constant disturbance can be found. Despite the unknown disturbance, the control system makes the system track the reference command. Figure 9 shows the three-dimensional trajectories of the sight vector of each satellite relative to the virtual structure, which is the result of the third stage, targeting or pointing toward a single target. Projection views of Fig. 9 onto the x–y, y–z, and z–x planes are shown in Fig. 10. Figure 11 illustrates the changes in the position and attitude of each satellite with a sequence of snapshots. As shown in Figs. 7–11, the virtual structure finds an efficient path to reorient its bore sight vector to the desired direction. Figures 12–14 show the control input histories of each satellite, and the input signal is within the acceptable range. In Fig. 12, satellite A uses more control resources to compensate for the effect of the unknown disturbance from 30–80 s. Figure 15 shows the result of the lumped uncertainty estimation by using Eq. (55). All the components of the estimated uncertainty vector are bounded and converged to certain values. Figure 16 shows the tracking error of satellite A. There are fluctuations due to the unknown disturbance, but the errors are properly converged to the

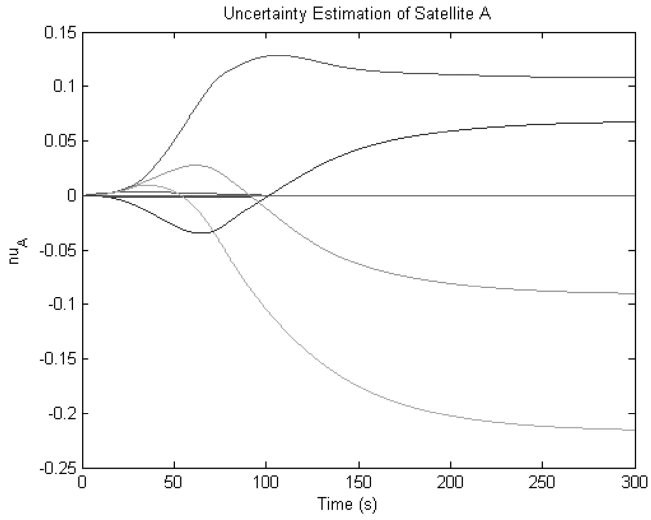

Fig. 15 Uncertainty estimation of satellite A.

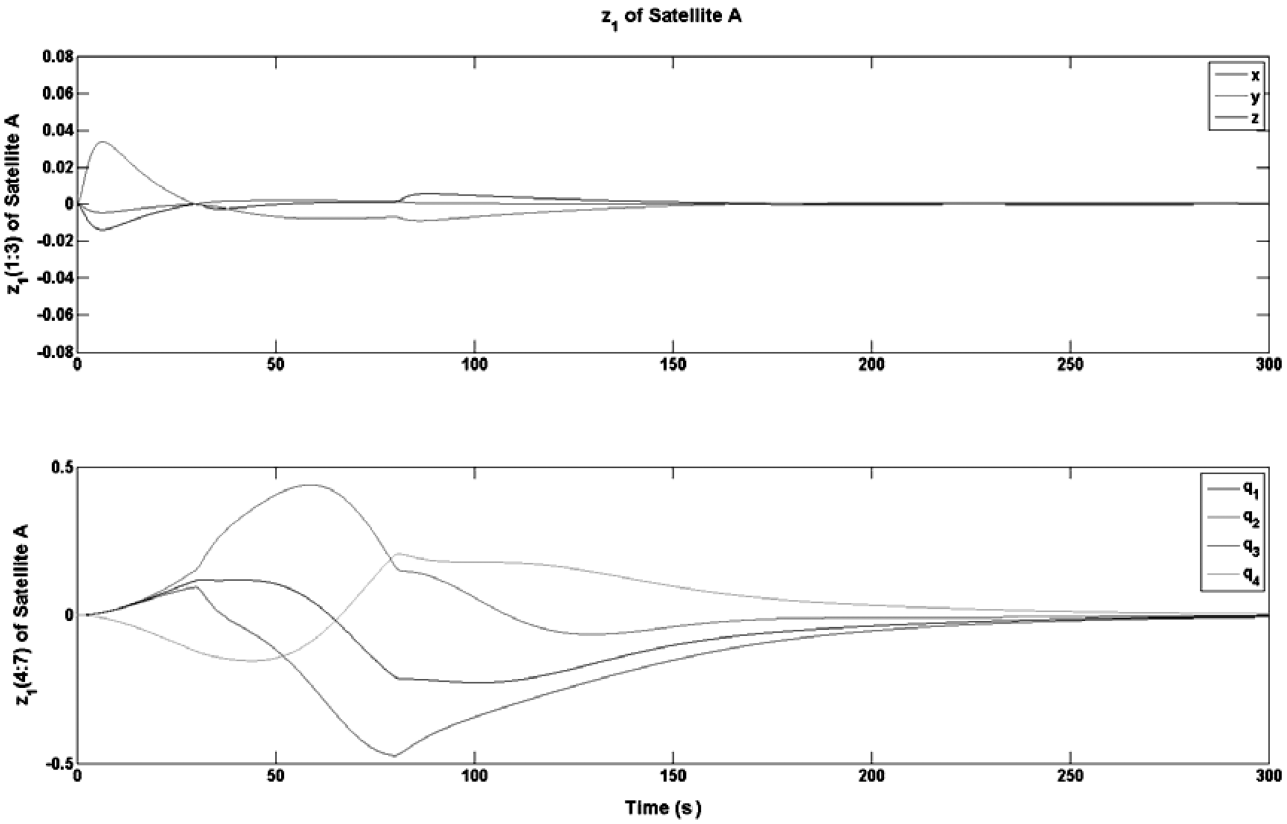

Fig. 16 Tracking error of satellite A.

desired value. The pointing target mission is completed in about 300 s. By properly designing the command filter for a mission, the thrust level can be reduced with a large mission time. Note that the pulse modulator, such as the Schmidt trigger, pulse width modulator, pulse width pulse frequency, etc., is required to produce on–off thrust firings for real implementation.

In summary, by applying the proposed formation flight scheme, each satellite is able to point toward the desired target correctly, and the virtual structure is maintained throughout the maneuver.

VI. Conclusions

This paper presented a formation flight control scheme based on the virtual structure technique. With the proposed formation flight scheme, a number of satellites can point toward the target simultaneously. The only required information for the formation maneuver is the position vectors of each satellite and of the target. From the position vectors, the proposed formation flight algorithm can calculate the required move displacement and rotation angle. The desired rotation angle is given by the desired quaternion, and the adaptive sliding mode controller is used to track the formation flying command.

The systematic design method of the adaptive sliding mode control scheme was developed for application to the formation flying command tracking control problem of satellites. The adaptive sliding mode control law and adaptive estimation law were derived, and a stability analysis was performed using the Lyapunov approach. The convergence of the estimated parameter error was also discussed. The proposed adaptive sliding mode control system showed the advantage of robustness for both parameter variations and time-varying disturbances. A numerical simulation was conducted to evaluate the effectiveness of the proposed virtual structure formation algorithm and the adaptive sliding mode control system. The simulation results showed the effectiveness of the proposed formation flight algorithm. This algorithm can be applied to various missions, such as the observation of the Earth's surface, space energy transmission, three-dimensional photographing of a target, and astronomical observation missions.

Acknowledgment

This work was supported by the Korea Science and Engineering Foundation (grant no. R01-2006-000-10189-0 funded by the Korea government).

References

[1] Beard, R. W., Lawton, J., and Hadaegh, F. Y., "A Coordination Architecture for Spacecraft Formation Control," *IEEE Transactions on Control Systems Technology*, Vol. 9, No. 6, 2001, pp. 777–790. doi:10.1109/87.960341

[2] VanDyke, M. C., and Hall, C. D., "Decentralized Coordinated Attitude Control Within a Formation of Spacecraft," *Journal of Guidance, Control, and Dynamics*, Vol. 29, No. 5, 2006, pp. 1101–1109. doi:10.2514/1.17857

[3] Leitner, J., Bauer, F., Folta, D., Carpenter, R., Moreau, M., and How, J., "Formation Flight in Space: Distributed Spacecraft Systems Develop New GPS Capabilities," *GPS World*, Vol. 13, No. 2, 2002, p. 22.

[4] Ren, W., and Beard, R. W., "Decentralized Scheme for Spacecraft Formation Flying via the Virtual Structure Approach," *Journal of Guidance, Control, and Dynamics*, Vol. 27, No. 1, 2004, pp. 73–82. doi:10.2514/1.9287

[5] Xin, M., Balakrishnan, S. N., and Pernicka, H. J., "Position and Attitude Control of Deep-Space Spacecraft Formation Flying via Virtual Structure and *θ-D* Technique," AIAA 2005-6090, Aug. 2005.

[6] Hammer, J., Piper, G., Thorp, O., and Watkins, J., "Investigating Virtual Structure Based Control Strategies for Spacecraft Formation Maneuvers," AIAA 2004-4898, Aug. 2004.

[7] Malla, R., Watkins, J., and Piper, G., "Study of Pointing Maneuvers for a Spacecraft Virtual Structure Formation," *The 38th Southeastern Symposium on System Theory*, Inst. of Electrical and Electronics Engineers, New York, March 2006, pp. 99–103.

[8] Lin, F. J., Shen, P. H., and Hsu, S. P., "Adaptive Backstepping Sliding Mode Control for Linear Induction Motor Drive," *Electric Power Applications*, Vol. 149, No. 3, 2002, pp. 184–193. doi:10.1049/ip-epa:20020138

[9] Wong, H., Kapila, V., and Sparks, A. G., "Adaptive Output Feedback Tracking Control of Spacecraft Formation," *International Journal of Robust and Nonlinear Control*, Vol. 12, Nos. 2–3, 2002, pp. 117–139. doi:10.1002/rnc.679

[10] Xu, Y., Tatsch, A., and Fitz-Coy, N. G., "Chattering Free Sliding Mode

Control for a 6 DOF Formation Flying Mission," AIAA 2005-6464, Aug. 2005.
[11] Wie, B., *Space Vehicle Dynamics and Control*, AIAA, Reston, VA, 1998, Chap. 5.
[12] Krstic, M., Kanellakopoulos, I., and Kokotovic, P., *Nonlinear and Adaptive Control Design*, Wiley, New York, 1995, Chap. 3.
[13] Khalil, H. K., *Nonlinear Systems*, 3rd ed., Prentice Hall, Upper Saddle River, NJ, 2002, Chap. 14.
[14] Ioannou, P. A., and Sun, J., *Robust Adaptive Control*, Prentice–Hall, Upper Saddle River, NJ, 1996, Chap. 3.